Semicond. Sci. Technol. **19** (2004) 1240–1249 PII: S0268-1242(04)77225-9

Carrier-density-wave transport and local internal electric field measurements in biased metal-oxide-semiconductor n-Si devices using contactless laser photo-carrier radiometry

Andreas Mandelis[1,2,4], **Micha Pawlak**[1,3] and **Derrick Shaughnessy**[2]

[1] Experimental Physics III, Solid State Spectroscopy, Ruhr-University Bochum, Universitaetsstr. 150, 44780 Bochum, Germany
[2] Center for Advanced Diffusion-Wave Technologies (CADIFT), Department of Mechanical and Industrial Engineering, University of Toronto, Toronto M5S 3G8, Canada
[3] Institute of Physics, Nicolaus Copernicus University, Grudziadzka 5/7, 87-100 Torun, Poland

E-mail: mandelis@mie.utoronto.ca

Received 4 March 2004
Published 16 September 2004
Online at stacks.iop.org/SST/19/1240
doi:10.1088/0268-1242/19/11/005

Abstract
Laser infrared photo-carrier radiometry was used with an n-type Si metal-oxide-semiconductor (MOS) diode and with a Si–SiO_2 structure with a transparent electrode and under external bias. Application of three-dimensional PCR theory yielded values of the minority carrier (hole) transport properties in the presence of the thus created local internal electric field at fixed frequencies. Furthermore, the internal electric field at fixed applied voltage was calculated. Under the combination of increased temperature and voltage, the sub-interface position of the carrier-density-wave centroid was found to depend on a trade-off between increased recombination lifetime and decreased ambipolar (conductivity) mobility. The ability of PCR to measure local internal electric fields by combining applied bias sweeps and frequency scans appears to pave the way towards the contactless reconstruction of depth profiles of these fields in active devices.

1. Introduction

The development of characterization strategies capable of evaluating the effects of the bulk substrate Si properties on the performance of microelectronic devices is an issue of growing importance, as evidence is accumulating that the electronic properties of the bulk can seriously affect the electrical characteristics of the device [1]. A case in point is the well-known compromising of the carrier diffusion length by the presence of Fe contaminants in B^+-doped p-type silicon where the formation of Fe–B pairs and the subsequent thermal or optical dissociation of the pairs leads to interstitial Fe and substitutional B with a concomitant reduction in the diffusion length [2–4]. Among the large number of available techniques [5], those that are contactless, such as surface protovoltage (SPV) [6, 7], have attracted much attention due to their non-intrusive character and their ability to monitor electrically the surface region of metal-oxide-semiconductor (MOS) structures. The existing contactless methods are, however, mostly steady-state techniques and

[4] On leave from: CADIFT.

therefore not depth-profilometric. For example, SPV is limited to monitoring the near-surface region of a structure, primarily the space-charge layer, or it probes the entire thickness of a wafer through the measurement of the steady diffusion length, $L_{dc} = (D_j\tau_j)^{1/2}$, where D_j is the minority (j) carrier diffusion coefficient and τ_j is the minority carrier recombination lifetime [6]. Recently, attempts have been made to extend the capabilities of SPV towards epitaxial layer lifetime characterization by introducing harmonic optical excitation and studying the frequency dependence of the SPV amplitude and phase as a function of lifetime, temperature and doping concentration of the epi layer among other parameters [8]. These efforts are still in their early stages. Nevertheless, although contactless in nature, SPV requires the presence of a charged transparent electrode a short distance away from the surface acting as a Kelvin probe, which can potentially interfere with electrical measurements of the device and would require stringent mechanical control for the implementation of scanning imaging technologies. Overall, SPV is intrusive to some extent, requires highly accurate control of the electrode-to-surface distance and suffers from low spatial resolution, as the size of the electrode becomes the limiting factor even with well-focused laser beams. On the other hand, modulated laser photothermal techniques have been used successfully for some time to probe semiconductor and device substrates [9, 10] through the optical generation and detection of free-carrier density waves (CDW) [11]. The interpretation of the photothermal or photoacoustic data is, however, quite complicated, as it involves a series of energy conversion pathways from optical to electronic, thermal and/or acoustic. As a result, the uniqueness of the measurements and mechanisms has come to question and these methods have found limited acceptance within the microelectronic device community, although they hold serious promise for laser-spotsize-limited spatial resolution, large range of depth profiles and non-contact, non-intrusive depth profilometry of the carrier transport properties in substrates [12] and in active devices [13].

In view of these limitations, the recently introduced technique of laser photo-carrier radiometry (PCR) has the advantage of spectrally filtering out all thermal and other interfering radiative emissions from photo-excited semiconductors and uses a narrow spectral window to detect near-bandgap infrared emissions solely originating with the recombining free-carrier-density wave. In Si, PCR originates in the form of infrared photon recombination emission (photoluminescence) at room temperature and above [14]. Using this method it was shown that very deep sub-surface defects, as far away as the back surface of a Si wafer, can compromise the electronic transport in the very-near upper surface region where devices are fabricated [14]. In this paper, we report the use of PCR in the monitoring of the effects of externally applied bias on CDW transport in an n-type MOS structure. The photogenerated CDW in n-Si is used as the probe of electronic transport at various distances below the $Si–SiO_2$ interface (‘sub-surface ranging’), via the frequency-dependent minority carrier ac diffusion length $L_{ac}(\omega) = L_{dc}/(1 + i\omega\tau_p)^{1/2}$. This complex quantity can vary greatly in the frequency range between dc and 1 MHz, typically used for Si probing due to the relatively long recombination lifetimes associated with modern-day wafers. At 100 Hz, the magnitude $|L_{ac}(\omega)|$ in n-type material with recombination lifetime $\tau_p \sim 1$ ms and $D_p \sim 12$ cm^2 s^{-1} [15], is approximately equal to 1 mm, and at 100 kHz it shrinks down to 14 μm. Given that the PCR signal is proportional to the depth integral of the CDW [14], under laser excitation in the blue-green spectral range where, for Si, the absorption coefficient $\alpha > 10^3$ cm^{-1} and $\alpha|L_{ac}(\omega)| \gg 1$ (optically opaque limit), the expression for the PCR signal in one dimension [11] exhibits optical photo-carrier saturation (i.e. independence from α), and simplifies to

$$S(\omega) \propto \frac{I_0 L_{ac}(\omega)}{2h\nu}\left\{\frac{(1-e^{-L/L_{ac}(\omega)})^2}{1+\left[\frac{(D^*/L_{ac})-S_1}{(D^*/L_{ac})+S_1}\right]e^{-2L/L_{ac}(\omega)}}\right\}, \qquad (1)$$

where I_0 is the incident laser intensity at optical frequency ν, L is the sample thickness, D^* is the ambipolar diffusion coefficient and S_1 is the front-surface recombination velocity. In deriving equation (1) the assumption was made that the back-surface recombination velocity is infinite. This is quite reasonable for the matte surface of industrial Si wafers (usually $S_2 > 10^3$ cm s^{-1} [16]). It is seen that in the electronically thick range (high frequencies), where $e^{-L/L_{ac}(\omega)} \ll 1$, the PCR signal is essentially proportional to the ac diffusion length and thus it exhibits simple depth ranging properties as the CDW probes different depths with changing modulation frequency. This property can be very useful for monitoring deep sub-surface carrier transport mechanisms subject to local electronic conditions, such as the local internal electric field, by means of the changes in the location of the statistical ‘centre-of-charge’, or ‘centroid’, of the CDW induced by external electric fields perpendicular to the surface and subject to sub-surface shielding by internal electric fields [17]. In turn, this information may be used to characterize hard-to-measure local electric field depth profiles in MOS and other device structures in open circuit configurations which normally can be probed neither electrically, impeded by lack of current or by current integration over the full thickness of the wafer, nor optically, impeded by opaque surface metallization and the non-profilometric nature of optical signals. In this paper, we show that sideways probing of opaque MOS structures with a super-bandgap laser beam focused at, or near, the rim of the metal plate produces carrier-density waves in the optically opaque Si which can probe deep sub-surface internal electric fields by virtue of the effects of the latter on the local CDW transport properties. The operator-adjustable ac diffusion length plays the role of a free-carrier probe of the sub-plate $Si–SiO_2$ interface and in the bulk region underneath the surface metallization which is impossible to interrogate with direct illumination. When detected by the PCR technique under external bias driving the MOS structure into depletion and inversion, the CDW is shown to yield a wealth of information about the magnitude of local electric fields and recombination processes at sub-surface depths selected by fixing the modulation frequency of the laser intensity.

2. Materials, devices and experimental results

A 10–15 Ω cm, 600 μm thick, n-type Si wafer was oxidized with a gate oxide of about 5000 Å and was subsequently front metallized with 1 mm diameter Al field plates (dots)

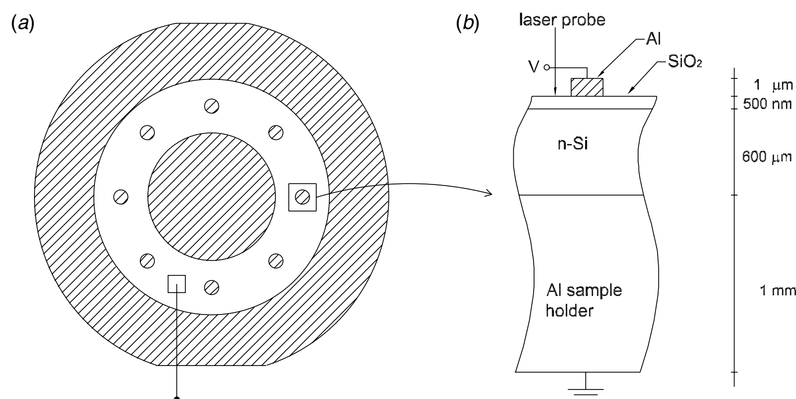

Figure 1. (*a*) Top view of 10–15 Ω cm n-type Si wafer used in MOS diode experiments. Cross-hatched areas: aluminium metallization including Al dots within the exposed SiO_2 area. Blank areas: SiO_2. Solid square with outward extended line: removable conducting transparent indium tin oxide (ITO) electrode connected to a voltage source. Dashed square: top-down view of the cross-sectional side view (*b*) (not shown to scale).

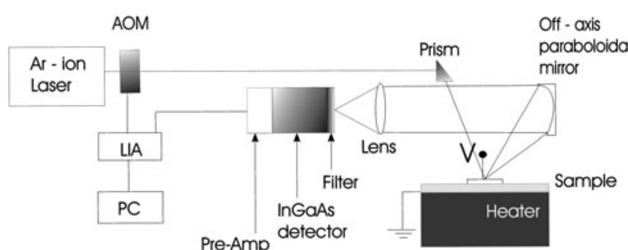

Figure 2. Experimental set-up for MOS device probing with PCR. The case of a transparent indium tin oxide (ITO) electrode on SiO_2 is shown. In the case of an MOS diode the laser beam is focused on the oxide at the rim of the device metal plate.

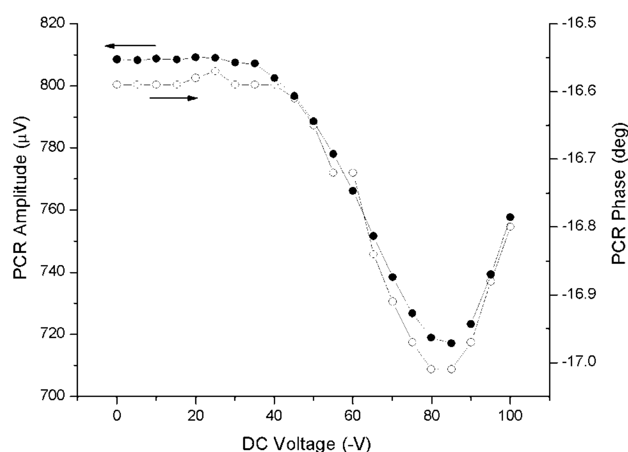

Figure 3. PCR amplitude and phase as a function of negative bias applied to the transparent electrode covering the SiO_2 layer adjacent to the location of Al dot gate in figure 1. Laser power approx. 100 mW at 514 nm; $T = 24$ °C.

to form MOS diodes. Otherwise, the SiO_2 layer remained exposed. Top and cross-sectional views of the wafer are shown in figure 1. The photo-carrier radiometry set-up is shown in figure 2. The IR detector was a switchable-gain InGaAs element (ThorLabs model PDA400), 1 mm in diameter, with spectral response in the 800–1750 nm range, peak response at 1550 nm and frequency bandwidth from dc to 10 MHz. The preamplifier was incorporated into the detector housing, a design which delivered optimal signal-to-noise ratio expressed as a NEP figure of $2.9–8.2 \times 10^{-12}$ W $Hz^{-1/2}$. The detector was outfitted with a specialty long-pass optical filter from Spectrogon featuring very steep cut-on (5% at 1010 nm, 78% at 1060 nm and a transmission range of 1042–2198 nm). The cut-on quality of the filter is crucial in PCR as it must block any pump radiation leakage from reaching the highly sensitive detector. Short-wavelength filtering of optical density 5 or 6 is usually required. The samples were placed on an aluminium backing which acted as a support, heater and signal amplifier by redirecting the forward emitted IR photons back towards the detector [14], figure 2.

Since the laser beam cannot penetrate the Al field plate of the MOS diode, two types of experiments were conducted: as a reference, one experimental configuration was with the laser beam directly on top of the exposed SiO_2 layer on the same wafer which was contacted with a removable conducting transparent indium tin oxide (ITO) electrode connected to a voltage source. The other configuration was with the laser light incident on the oxide on the side of an Al dot (figure 1(*b*)) and at an adjacent region to the (removed) transparent electrode. The metal plate was biased by means of a metallic needle. The aluminium sample holder was connected to the electrical ground in an open circuit configuration and negative potentials were applied to the upper electrode, so as to drive the n-type device into depletion and a thin Si–SiO_2 interface layer into inversion [18]. Electric fields nominally up to 1.7 kV cm^{-1} normal to the surface were thus obtained. With the entire back surface of the wafer at ground potential, in the case of the MOS structure the electric field lines tend to spread out away from the biased metal plate to some extent [19], thus nearly equalizing the local sub-surface electric field intensity between the sub-plate and probe regions. Most importantly, the long CDW diffusion lengths of carriers generated by the laser beam in the Si substrate through the transparent oxide near the metal plate rim (∼200 μm) were able to probe and sample the electrical landscape well underneath the dark sub-plate region. In the case of the contacting transparent electrode, its large size compared to sample thickness generated field lines normal to the wafer surface at the measurement location. Figures 3 and 4 show the behaviour of the PCR signal in each of these

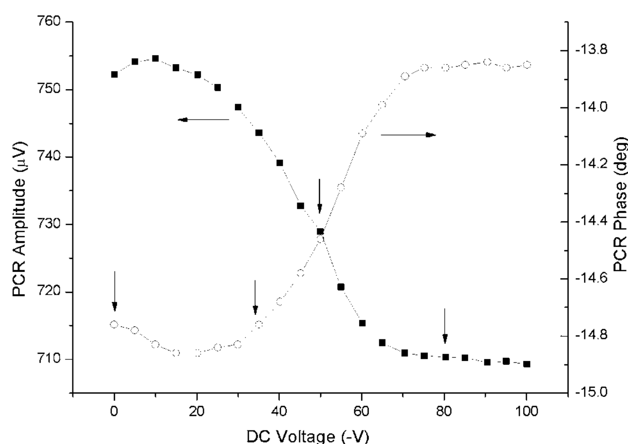

Figure 4. PCR amplitude and phase as a function of negative bias applied to the aluminium gate of the n-type MOS structure. Laser power approx. 100 mW at 514 nm; $T = 24$ °C. The vertical arrows indicate potentials at which frequency scans were performed.

two configurations as a function of applied bias at 5 kHz. This frequency was used because it yielded a large enough carrier diffusion length (~200 μm) for probing the under-the-Al plate region and an acceptable signal-to-noise ratio. While the MOS diode data were very reproducible, it was found that in order to obtain reproducible data with the removable transparent electrode it was necessary to cycle the electric field at least once in the beginning of measurements. This is very likely due to charge transfer effects from the biased electrode to the oxide which needed to be saturated before measurements could be made. After cycling, the final profiles versus applied voltage, but not the signal levels, were similar albeit shifted on the V axis, to those obtained using an insulating mica sheet (about 30 μm thick) between electrode and oxide to prevent charge transfer. However, the signal-to-noise ratio with the mica sheet was considerably worse because the effective electric field intensity was greatly diminished. Laser-beam modulation frequency scans of the MOS structure were also performed at fixed bias as indicated by the vertical arrows in figure 4, in order to extract quantitative information about the photo-carrier transport properties, as will be detailed in section 3.2. The instrumental transfer function of the system was determined very simply by allowing a small amount of scattered laser light to reach the InGaAs detector. By modulating the scattered light intensity the instrumental amplitude and phase frequency responses were obtained and used to normalize the PCR amplitudes through division and the phases through subtraction.

The PCR signals from both semiconductor structures exhibit decreasing amplitudes with increasing negative bias. However, at large negative biases the directly illuminated interface exhibits a minimum at about −80 V, figure 3. The PCR phase *lag* also tends to follow closely the amplitude behaviour, first increasing and then turning around above −80 V to reach smaller values. In the sideways illuminated MOS structure, figure 4, the amplitude tends to saturate at a low value at, or above −80 V, however, the phase is strictly anti-correlated. It is worth noting that the PCR phase resolution in these measurements is excellent, of the order of 0.03° or better. This level of resolution is important when measurements of the

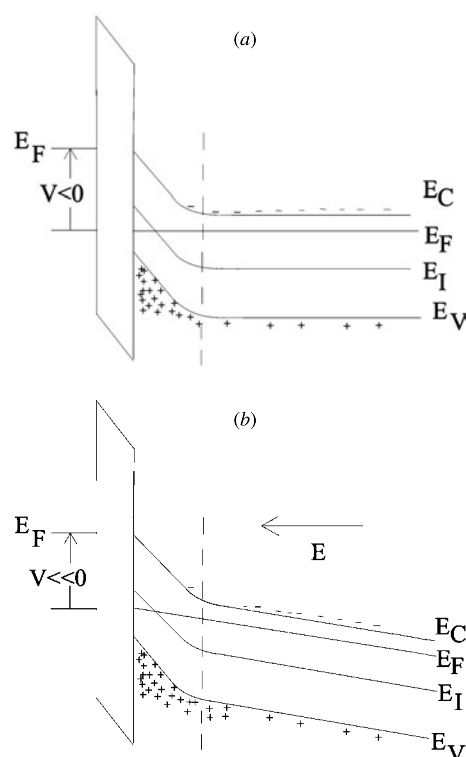

Figure 5. Energy band diagram of n-type Si MOS diode in depletion/inversion. E_C: conduction-band edge; E_F: Fermi level in both semiconductor and metal; E_I: intrinsic Fermi level in the semiconductor; E_V: valence-band edge. (*a*) $V < 0$; (*b*) $V \ll 0$.

sub-surface shift of the minority CDW distribution (centroid) are made due to the subtle nature of this effect on account of the well-known shielding effects of internal electric fields. When positive potentials were applied, there was no change in the PCR signals from their $V = 0$ values in either configuration. Similar behaviour (with the opposite polarity) was observed with p-type 1–5 Ω cm oxidized wafers, but is not reported here.

3. Theory and discussion

3.1. Carrier-density-wave charge centroid separation under bias

For direct super-bandgap laser photon incidence on the negatively charged SiO_2–Si interface under the transparent ITO electrode, the Si surface is most definitely inverted, forming a field-induced p–n junction in an n-type substrate [18, 20]. Figure 5(*a*) depicts the situation for moderate applied fields (semiconductor bulk flat bands); figure 5(*b*) shows the situation for large applied fields ($V \ll 0$) where a part of the potential drops across the body of the semiconductor, thus tilting the bands beyond the space-charge layer (SCL) edge and accelerating the motion of free carriers. At zero external field, there exists a residual SCL due to uncompensated electronic charge trapped (embedded) in the oxide at the SiO_2–Si interface. Detailed charge neutrality around the interface requires an equal amount of charge of the opposite sign to be accumulated on the other (Si) side of the interface which gives rise to the SCL. The laser injects a harmonically modulated

excess carrier-density wave which effectively forward-biases the interface and decreases the SCL width. The latter oscillates between a maximum (dark) and minimum (full light exposure) value at $V = 0$ and the PCR signal represents a reference value for the electronic state of the interface. The boundary-value problem governing the free photoexcited excess carrier (electron–hole pair, ehp) density $\Delta N(x; \omega, E)$ responsible for the PCR signal in one dimension is [11]

$$D\frac{\mathrm{d}^2\Delta N(x;\omega,E)}{\mathrm{d}x^2} - K_\mathrm{e}^2\Delta N(x;\omega,E) = -\frac{\beta(1-R)I_0}{2}\,\mathrm{e}^{-\beta x} \tag{2a}$$

subject to boundary conditions

$$\left.D\frac{\mathrm{d}\Delta N(x;\omega,E)}{\mathrm{d}x}\right|_{x=0} = S_1\Delta N(0;\omega,E),$$
$$\left.D\frac{\mathrm{d}\Delta N(x;\omega,E)}{\mathrm{d}x}\right|_{x=L} = -S_2\Delta N(L;\omega,E) \tag{2b}$$

where D, S_1 (S_2) are the ambipolar diffusivity, and the front-(back-) surface recombination velocity. K_e is the carrier wavenumber in the presence of an *internal* electric field E and is explicitly given by equation (4). R is the reflectance of the semiconductor surface at the excitation wavelength, β is the optical absorption coefficient at the same wavelength and ω is the angular modulation frequency of the laser-beam intensity. For a fixed modulation frequency, the phase lag of the system increases as the applied voltage increases above a threshold value required to change the local electric field in the semiconductor bulk and induce electron–hole separation beyond the $V = 0$ configuration. This occurs because the negative bias increasingly repels the majority CDW distribution (electrons) pushing them deeper into the bulk. A measure of this drift is the CDW statistical centroid, which can be defined as

$$\langle x(\omega,E)\rangle = \left|\int_0^L x\Delta N(x;\omega,E)\,\mathrm{d}x\right| \Big/ \left|\int_0^L \Delta N(x;\omega,E)\,\mathrm{d}x\right|. \tag{3}$$

Here E is the local internal electric field which depends on the crystalline band structure, on impurities and defect configurations. It changes with the motion of free charged particles and interacts with them. It is also affected by the value of the external field which drives carrier motion in a complicated way. The boundary-value problem (2) results in a solution $\Delta N(x; \omega, E)$ which involves spatially decaying contributions from infinite reflections of the carrier-density wave from the two surfaces. Assuming that the back surface of the wafer is an effective recombination site for carriers, under the applied negative field and reverse-bias conditions [18], all interreflection terms but the first forward contribution vanish and the CDW distribution function can be simply written as [11]: $\Delta N(x; \omega, E) = \text{const} \times \mathrm{e}^{-K_\mathrm{e}x}$, where the CDW wavenumber is

$$K_\mathrm{e}^{\pm}(\omega,E) = \sqrt{Q^2(E) + L_\mathrm{ac}^{-2}(\omega)} \pm Q(E);\quad Q(E) \equiv \mu^* E/2D^*. \tag{4}$$

Here μ^* is the ambipolar mobility. The (+) sign is associated with the minority carrier density wave which is attracted closer to the Si–SiO_2 interface resulting in a narrower spatial distribution than without external bias. The (−) sign is associated with the majority carrier density wave which is repelled by the external bias, resulting in a broader spatial distribution than without bias. Therefore, the applied field effectively separates out the minority and majority CDW distributions, with electron density heavily depleted from the inverted interface under the steepened energy bands, as it increases the SCL width and tilts the bands beyond its boundary. For high enough modulation frequencies so that the semiconductor is electronically thick, the CDW centroid is found to be simply:

$$\langle x\rangle_{\pm} \approx 1/K_\mathrm{e}^{\pm}(\omega,E). \tag{5}$$

This quantity can be further used to describe the *relative* separation between the positive and negative charge density diffusion-wave centroids

$$\langle\Delta x(E,\omega)\rangle = \langle x\rangle_- - \langle x\rangle_+ = 2Q(E)L_\mathrm{ac}^2(\omega) = \frac{v_\mathrm{d}\tau_\mathrm{p}}{\sqrt{1+(\omega\tau_\mathrm{p})^2}} \tag{6}$$

where $v_\mathrm{d} = \mu^* E$ is the ambipolar drift velocity under the influence of the internal electric field. The value of E implicitly takes into account the generation of an opposing electric field near the back surface of the semiconductor at open circuit due to the accumulating negative charge at high external biases. The result of this accumulation would be a more effective shielding of the external electric field $E_\mathrm{ext} = V/d$ by the internal field. Nevertheless, the minority and majority CDW centroids drift further apart with increasing external electric field which in turn increases the local electric force, and/or with decreasing modulation frequency (i.e. increasing L_ac), which tends to amplify the effects of the very different mobilities of electrons and holes on the drift of the respective centroids apart. Frequency, of course, has no effect on separation when $\omega\tau_\mathrm{p} \ll 1$. Owing to the increased separation of the centroids, the radiative recombination probability of photoinjected holes into occupied impurity states of the doped semiconductor decreases, as holes are confined mainly in the SCL in the neighbourhood of unoccupied impurity states. At the same time depleted majority electrons accelerate into the quasi-neutral region to occupy impurity states deeper into the semiconductor. This results in decreased PCR amplitude as only the exponentially decreasing tail end of the coherently oscillating free-hole density overlaps the proximity of the majority CDW centroid for recombination into occupied impurity states and NIR photon emission [21]. This is accompanied by an increased phase lag, figure 3, indicating the shift of the recombination site deeper in the Si substrate with $V < 0$. As $V \ll 0$, the degree of inversion in the very-near-surface region increases with the increased density of photo-excited coherently oscillating holes due to their spatial confinement. For typical SCL widths of <1 μm in Si, and optical absorption length α^{-1}(514 nm) ≈ 1 μm, most ehp are generated inside the SCL. At a critical value of the bias in the range of −80 V, the effectiveness of the strong SCL band-bending in separating the photo-generated electron–hole pairs through drift motion of the electrons into the quasi-neutral region decreases as large numbers of hole states become available at energies below the top of the valence band within

the SCL. Besides, the negative charge builds up in the bulk to slow down the acceleration of electrons away from the $Si–SiO_2$ interface. These effects result in a concomitant increase in radiative recombination probability within the SCL and emission of NIR photons from the interface region. Accordingly, the PCR amplitude starts to increase above -80 V and the phase lag decreases as SCL recombination moves the statistical photon emission centroid closer to the $Si–SiO_2$ interface from the bulk. The fact that there was no measurable PCR signal change from the $V = 0$ value under applied positive bias is an additional indication that the drift of the majority CDW away from the interface does not control the generation of the PCR signal which appears to depend solely on the recombining minority carriers as the source of IR photon emission.

Now turning to figure 4 which shows results with the laser beam on the oxide just beyond the rim of the metal plate of the biased MOS structure, the change in PCR signal from its $V = 0$ value is, again, associated with the depleting $Si–SiO_2$ interface directly below the metal plate. Given the relatively high optical absorption coefficient of Si at 514 nm, photons can only illuminate directly about 1 μm of the sub-plate region ('leakage photons'). Therefore, it is carrier-density waves generated at the location of the laser beam which coherently diffuse and probe distances commensurate with $L_{ac}(\omega)$, equation (1), under the metal plate and the oxide layer where they are affected by the internal electric field E. Unlike the case of direct illumination through the transparent electrode, the charge centroid of the sideways diffusing CDW is the same for both photo-generated electrons and holes as they enter the dark electric field region together (within a Dember factor owing to mobility differences, which yields negligibly small local separation potentials of the order of 10^{-8}–10^{-6} V [22]). When the CDW enters the biased sub-plate region from the side, where the internal field effects are strongest, it has already diffused as far as one $L_{ac}(\omega)$ away from the $Si–SiO_2$ interface in both depth and radial directions. This corresponds to a built-in phase lag at the boundary of the active sub-plate region at $V = 0$. As $|V|$ increases, separation of the opposite-sign CDW centroids commences, as described by equation (6). The decrease in PCR amplitude occurs for the same reasons as in figure 3, that is, the excess electric field efficiently separates out majority and minority carriers under inversion conditions. The recombining minority CDW (which is solely responsible for the generation of the PCR signal) moves closer to the depleted SCL attracted by the increasing negative electric field there, and thus closer to the laser source, yielding a decreasing phase lag at the same time as the radiative recombination probability decreases due to increasing centroid separation and diminished overlap. This leads to the observed anti-correlation between PCR amplitude and phase behaviour in figure 4. Measurements with an increased distance of the laser beam away from the Al plate rim have confirmed an increased phase lag at $V = 0$. Under inversion conditions in the SCL, the positive CDW eventually accumulates fully, saturating the position of the centroid and leading to the saturation of the PCR amplitude and phase channels. Because in the absence of direct surface illumination there is no ehp photo-generation within and beneath the SCL, there is no enhanced recombination possible there to lead to PCR signal inversion. At 5 kHz complete accumulation occurs for $|V| > 70$–80 V as shown in figure 4. Experiments at other frequencies showed that at 500 Hz gradual saturation sets in at $|V| > 90$–100 V. At 103 kHz complete saturation sets in for $|V| > 50$ V. These trends are fully consistent with the increased spatial confinement of the CDW at higher frequencies due to the shorter L_{ac}, leading to the narrowing of its spatial distribution which affects the position saturation of the respective centroid. The foregoing mechanisms of signal behaviour versus applied external field in the two configurations (transparent electrode-oxide-Si and MOS) hold qualitatively despite the different dimensionalities of the obtained PCR signals (the former configuration was one dimensional, the latter was three dimensional). In any case, even under focused laser photo-carrier generation in the MOS structure, the large diffusion length at 5 kHz tends to spread the CDW widely below the metal-plate region, largely conforming to one-dimensional behaviour with regard to relative positional changes of the CDW induced by the external bias.

3.2. CDW transport properties and internal electric field profiles

The normalized PCR amplitudes and phases at the prescribed voltages in figure 4 are shown in figure 6. The simulated geometry is that of figure 1(*b*). The three-dimensional PCR theory [14] was implemented numerically to yield the PCR signal integrated over the size (aperture) of the detector of radius A:

$$P(\omega) = \text{const} \times \int_0^A r\,\mathrm{d}r \int_0^L \Delta N(r, z; \omega)\,\mathrm{d}z, \tag{7}$$

with the free-carrier density $\Delta N(r, z; \omega)$ obtained from [11], chapter 9, equation (9.106), and reproduced here:

$$\begin{aligned}\Delta N(r, z, \omega) = \frac{\eta_Q P_0 \alpha}{2\pi h\nu D^*} \int_0^\infty \frac{\mathrm{e}^{-k^2W^2/4}}{(\alpha^2 - \xi_e^2)} \\ \times \left[\left(\frac{G_2 g_1 - g_2 G_1\,\mathrm{e}^{-(\xi_e+\alpha)L}}{G_2 - G_1\,\mathrm{e}^{-2\xi_e L}} \right) \mathrm{e}^{-\xi_e z} - \mathrm{e}^{-\alpha z} \right. \\ \left. + \left(\frac{g_1 - g_2\,\mathrm{e}^{-(\alpha-\xi_e)L}}{G_2 - G_1\,\mathrm{e}^{-2\xi_e L}} \right) \mathrm{e}^{-\xi_e(2L-z)} \right] J_0(kr) k\,\mathrm{d}k,\end{aligned}$$

where

$$\begin{aligned} g_1(k) &\equiv \frac{D^*\alpha + S_1}{D^*\xi_e(k) + S_1} \qquad & g_2(k) &\equiv \frac{D^*\alpha - S_2}{D^*\xi_e(k) - S_2} \\ G_1(k) &\equiv \frac{D^*\xi_e(k) - S_1}{D^*\xi_e(k) + S_1} \qquad & G_2(k) &\equiv \frac{D^*\xi_e(k) + S_2}{D^*\xi_e(k) - S_2}. \end{aligned} \tag{8}$$

Here, k is the Hankel variable of radial integration; W is the Gaussian laser beam spotsize (1/e); S_1 and S_2 are front- and back-surface recombination velocities; η_Q is the quantum yield for optical to electronic energy conversion for generation to carrier-density waves and P_0 is the laser power. The theory was modified to include an effective internal electric field E sampled by the photo-excited free carriers by replacing the conventional CDW wavenumber $\sigma_e(\omega) = L_{ac}^{-1}(\omega)$ with $K_e^+(\omega, E)$ of equation (4) for the minority CDW, so that

$$\xi_e(k; \omega, E) = \sqrt{k^2 + \left[K_e^+(\omega, E)\right]^2}. \tag{9}$$

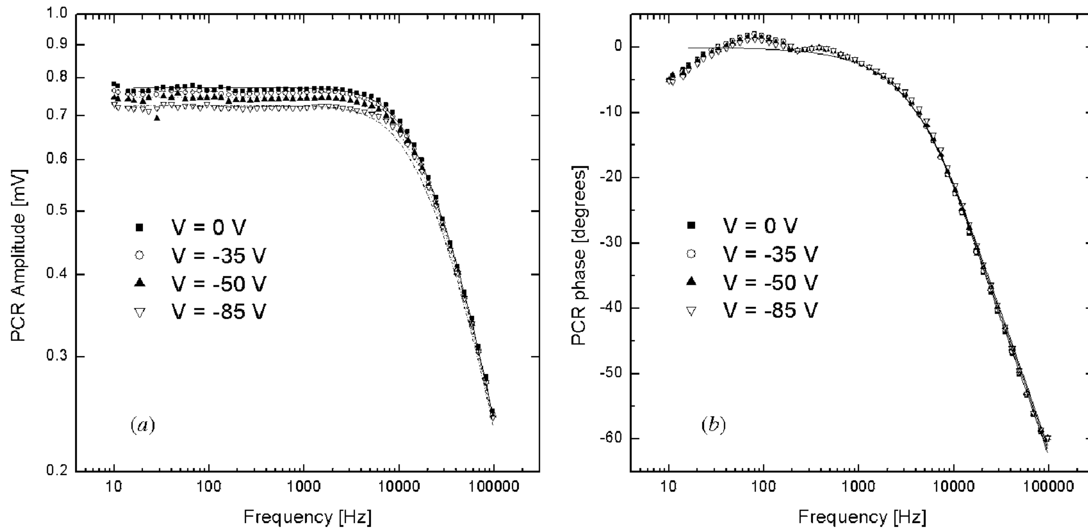

Figure 6. PCR frequency scans of the MOS diode under bias and theoretical fits. (*a*) Normalized amplitude; (*b*) normalized phase.

Table 1. CDW transport properties and internal (local) electric fields under external bias calculated from simultaneous best fits of equations (8), (9) to PCR amplitude and phase data.

$-V$ (V)	Q (cm^{-1})	τ_p (μs)	D^* (cm^2 s^{-1})	E (V cm^{-1})	Error (%)
0	0	28.50	27.80	–	2.9469
35	25	29.22	28.25	3.14	2.9519
50	100	26.77	27.99	12.57	2.7936
80	520	22.32	25.05	57.89	2.9374

It should be emphasized that the foregoing theory is strictly valid for a radially homogeneous distribution of photo-carriers, whereas the geometry of our MOS structures includes a lateral inhomogeneity with the presence of the top Al layer adjacent to the exposed oxide. Nevertheless, in view of the expected radial spreading (fanning out) of the electric field lines [19] and the long $L_{ac}(\omega)$ at frequencies up to 10 kHz ($\sim$100 μm), the degree of lateral electric field inhomogeneity is largely smeared out in the illuminated spot immediately next to the Al layer and the assumed homogeneity can be justified. An inhomogenous source aperture can be straightforwardly taken into account using the Green-function formalism of carrier-density waves [11], but the mathematical complexity would tend to obscure the essential physics of the problem which rests with the mechanisms of *relative* PCR signal variations with applied electric field magnitude. The essential agreement of the actual experimental diffusion-wave configuration with a laterally homogeneous geometry is further corroborated by the good fits of the frequency scans to the homogenous PCR theory, figure 6. The $V = 0$ curves were used as reference to obtain the best-fit values for $A = 150$ μm, our effective detector radius. The remaining three curves were fitted by allowing the value of Q as well as the values of the recombination lifetime, τ_p, and ambipolar diffusion coefficient, D^*, to vary in the fitting program so as to obtain the lowest possible error. The fitting results are shown in table 1. The values of the internal electric field were calculated from the fitted value of Q and its definition in equation (4). Since the ambipolar mobility is defined as

$$\mu^* \equiv \frac{(n_0 - p_0)\mu_n\mu_p}{n\mu_n + p\mu_p} \approx \mu_p \qquad (10)$$

for n-type Si with $n \approx n_0 \gg p$ (n_0 and p_0 denote equilibrium carrier densities), the value of the hole mobility at room temperature (450 cm^2 V s^{-1}) was used in those calculations. The slight increases in τ_p and in D^* for $V = -35$ V over the $V = 0$ value are consistent with the non-monotonic behaviour of the voltage scan below -30 to -40 V in figure 4. This trend was also observed for the 102.5 kHz scan. The trend was not observed with the scan using the transparent electrode. It may be due to the increased depletion of occupied impurity states under the repulsive electric field within the centroid overlap region at relatively low negative potentials and before the drift of the hole density wave seriously perturbs the recombination rate downwards. Such depletion would deprive free holes from potential recombination partners (trapped electrons) and would increase the effective minority carrier lifetime, at least the part of it associated with radiative recombination. The relatively short recombination lifetime values and high ambipolar diffusivities in n-type Si obtained from the fits of figure 6, compared to expected values in high-electronic quality substrates, point to a material with a large density of electronic traps, quite a common situation in metallized SiO_2–Si interfaces, leading to inordinately small contributions of the minority photo-carrier (holes) to the weighted diffusivity value represented by D^* which thus assumes values much closer to typical majority diffusivity ($\sim$30 cm^2 s^{-1}) as obtained in table 1. An additional cause of these values can be the photoinjection level: for a laser power of 200 mW on the sample at $W = 30$ μm, the optical injection flux was approx. 1.96×10^{17} cm^{-2} s^{-1}, and the injected carrier density was 2.1×10^{19} cm^{-3}. Typical low-injection levels are in the range of 10^{12}–10^{14} cm^{-3} [5,7]. At the high-injection level of our experiments recombination lifetimes of the photo-excited minority carriers can decrease significantly due to carrier–carrier scattering [5] thus also creating the conditions for ambipolar diffusivity domination by the high values of the majority electrons. The values of internal electric fields

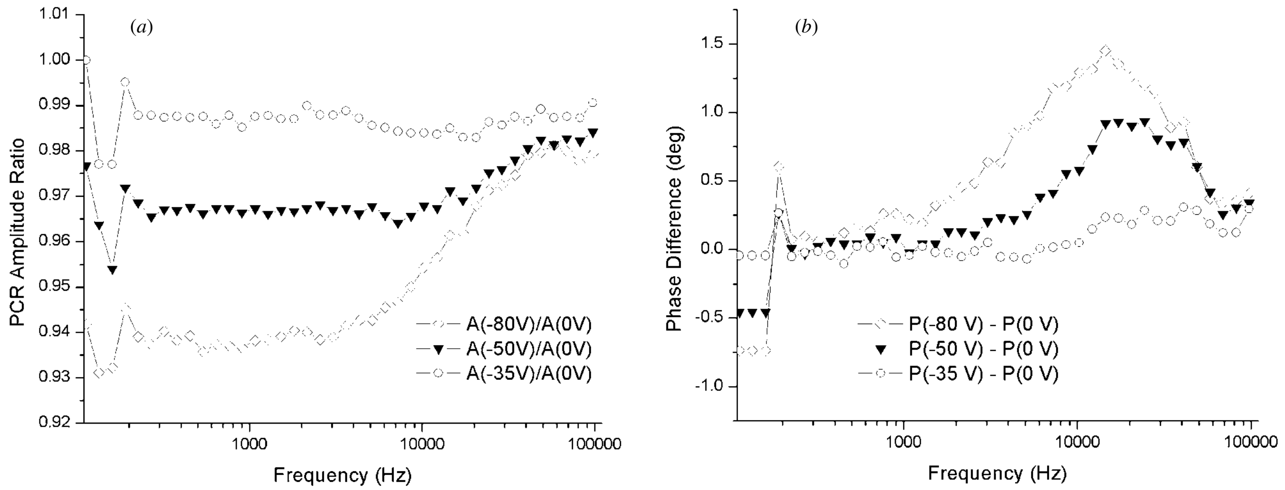

Figure 7. Frequency scans of relative PCR amplitude ratios (*a*) and phase differences (*b*) of biased MOS device at 24 °C.

estimated in table 1 through fitting are low compared to the externally applied field and well within the independently calculated range in the literature [17].

The compensation (self-shielding) of the internal electric field as the charge centroids separate out under bias saturates the maximum distance possible even under large external biases (up to -100 V), so that the field effect causes relatively small changes in the PCR signal frequency scan, as seen in figure 6. Equation 6 and table 1 predict a saturation distance of 470 μm at 5 kHz for $|V| \geqslant 80$ V, which places the oppositely charged CDW distributions near the opposite surfaces of the wafer, as expected. Besides the absolute amplitude and phase frequency scans, additional insights into the dynamics of the carrier wave under bias can be garnered by plotting the phase differences and amplitude ratios relative to the $V = 0$ reference state. These plots are shown in figure 7. The separation of the flat amplitude ratios at frequencies below ∼4 kHz away from the $V = 0$ (normalized value 1) in figure 7(*a*) shows that frequency-dependent CDW distribution shift and narrowing does not occur below $\omega\tau_p \approx 0.15$ and is consistent with equation 6. Figure 7(*b*) corroborates this conclusion showing little or no phase shift up to the same frequency range. The onset of CDW centroid separation clearly appears to occur in the 1–3 kHz range and the relative phase lag decreases under increasing bias, as expected, up to approx. 20 kHz. For higher frequencies all relative phases converge to the same value. Similar observations can be made about the amplitudes in figure 7(*a*). These are consequences of the fact that the generation point of the CDW field lies outside the location of the free hole-wave distribution below the Si–SiO_2 interface. For the measured transport parameters of table 1 and for frequencies up to 3 kHz, L_{ac}(1 kHz; -80 V) = 236 μm and L_{ac}(1 kHz; 0 V) = 277 μm. In this range the recombination kinetics and the intrinsic spatial overlap (in the limit of unmodulated optical excitation) of the centroids control the spread of the carrier wave. For $f > 3$ kHz, $\omega\tau_p$ ceases to be negligible for all minority recombination lifetimes in the range. Therefore, the centroid of the CDW is not controlled by the internal-field-dependent recombination dynamics deep in the sub-plate region, but rather by the decreasing shortest probe distance to the Si–SiO_2 interface from the measurement spot (the detector is focused at the laser beam intersection with the wafer surface). The shortened distance is dominated by near-surface SCL recombination, so there is no measurable phase lag. This is clearly further illustrated by the high-frequency behaviour of the relative amplitude curves in figure 7(*a*): they converge to the same value as the effects of diminished recombination with increasing centroid separation in the bulk begin to lie outside the reach of the PCR depth integral of the collected IR emissions [14] represented by equations (7) and (8), and the very-near-surface recombinations within the SCL dominate. It is concluded that modulation frequency scanning of the CDW corresponds to local internal electric field ranging within the ac diffusion length and it can be used to extract depth profilometric reconstructions of this quantity from complete frequency scans.

3.3. Temperature dependence of voltage scans

Voltage scans of the MOS structure were also performed at various elevated temperatures. The PCR behaviour of the structure under sideways illumination was very similar to our earlier results with n-type Si [23]: the absolute amplitude increased substantially with temperature and so did the phase lag. These trends are consistent with the Shockley–Reed mechanism [24] of increasing recombination lifetime and decreasing ambipolar diffusion coefficient. The effects of increased temperature on the CDW centroid drift are much more subtle in both amplitude and phase variations than the absolute changes in amplitude and phase because of the small magnitudes of the involved internal electric fields due to compensation (self-shielding). Therefore, the normalized curves of figure 8 were constructed to highlight the internal electric field effects. The functions plotted there are as follows:

Relative normalized amplitude:
$$R = \frac{A(T,V) - A(T_0,V)}{A(T,0) - A(T_0,0)} \tag{11}$$

Relative normalized phase:
$$\Delta\Phi = [\phi(T,V) - \phi(T_0,V)] - [\phi(T,0) - \phi(T_0,0)], \tag{12}$$

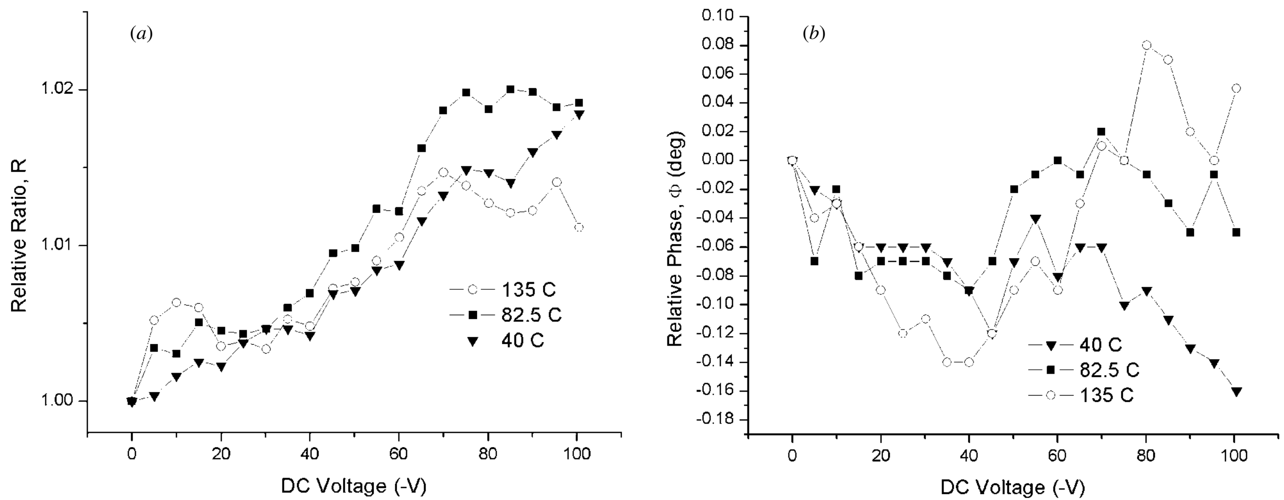

Figure 8. Relative normalized amplitudes (*a*) and phases (*b*), equations 11, 12, of voltage scans at various elevated temperatures of the MOS diode obtained at $f = 5$ kHz.

where $T_0 = 24\,^{\circ}$C. These curves represent the relative departure of the PCR signal from its value at room temperature and at zero electric field. The signal-to-noise ratio for each absolute curve used for the relative profiles was a minimum of 811–850. This yields error bars on the order of 0.001–0.0015 for the relative amplitudes of figure 8(*a*) and 0.0012–0.0015 degrees for the relative phases of figure 8(*b*). Using standard thermal-wave theory in three dimensions it was found that at the centre of the incident laser beam ($r = 0$) the maximum ac temperature rises, given by [25]

$$T(0, 0; \omega) = \frac{\sqrt{\pi} W I_0}{\Lambda} \exp(\sigma^2 W^2/4)\, \mathrm{erf}c(\sigma W/2) \qquad (13)$$

is only 2–3 K. Here Λ is the thermal conductivity of Si (=150 W mK^{-1}), and σ is the thermal wavenumber, $\sigma = \sqrt{\mathrm{i}\omega/\beta}$, and β is the thermal diffusivity (=0.9 cm^2 s^{-1} for Si). Therefore, it was verified that the trends observed in figure 8 are due to the changing temperature of the Si lattice with minimal or no heating effects from the laser beam. There are opposing trends in the plots of figure 8: for instance, as recombination lifetime increases at elevated temperatures, the relative CDW centroid separation also tends to increase, however, mobility decreases, thus counteracting that tendency. Figure 8(*a*) shows that the overall relative PCR amplitude increases under bias at all elevated temperatures. This is consistent with the increased lifetime dominating the PCR response through the increased density of free photo-excited carriers [23]. Figure 8(*b*) also shows an increased relative phase lag up to approx. −40 V, also indicating that the CDW recombination centroid moves deeper into the bulk as intuitively expected from the increased carrier lifetime. The very small phase shifts with temperature can be understood in terms of the simple model of equation (6) with ambipolar mobility being the only temperature-dependent parameter: using parameters from table 1 and the accepted mobility temperature dependence for Si [26, 27]

$$\mu_{\mathrm{p}}(T) = 2.3 \times 10^9 T^{-2.7}\ \mathrm{cm}^2\ \mathrm{V}^{-1}\ \mathrm{s}^{-1} \qquad (14)$$

we find a relative carrier-wave centroid shift $\delta\langle\Delta x(E, w)\rangle \cdot 9.18 \times 10^{-5}(\Delta\mu^*)\,\mathrm{cm} = 20\ \mu\mathrm{m}$, with $\Delta\mu^* \sim \Delta\mu_{\mathrm{p}}$ being the change (decrease) in ambipolar mobility between 300 K and 400 K. This very small shift compared to the carrier diffusion length L_{ac} amounts to a small fraction of a degree only. Recall that the measurement of phase of the order of 0.01° is meaningful, as our PCR system is capable of resolving phases of 10^{-3} degrees. In any case, considering the relative relationships of amplitude and phase curves, figure 8, a more complicated picture emerges. Because the increasing τ_{p} facilitates a further increase in relative CDW centroid separation when $\omega\tau_{\mathrm{p}} < 1$, equation (6), above a critical temperature range which seems to be between 82.5 °C and 135 °C, the radiative recombination probability decreases when the internal electric field is large enough to efficiently separate out the CDW centroids *and* the temperature is high enough to decrease the intrinsic diffusivity and mobility through scattering with phonons and impurities. Using PCR we have shown that for n-type Si with resistivity 10–15 Ω cm, the fractional decrease in mobility between 300 and 550 K is greater than the fractional increase in recombination lifetime [23]. Therefore, it would appear that both mechanisms based on the T-dependence of lifetime and mobility, act to decrease the radiative emission rate from recombining free carriers in spatially overlapping regions. However, at the highest temperatures non-radiative recombination through scattering may be responsible for the relative PCR signal decrease. In figure 8(*a*) the R (135 °C) curve rises along with the other two curves at low V, but ends up below the other curves for potentials $|V| > 70$ V. Energy loss due to enhanced scattering promotes localization closer to the Si–SiO_2 interface and a larger relative phase lead. This can be the result of a significant decrease in the mobility of the minority carrier which controls the $\langle x(\omega, E)\rangle$, consistently with our earlier findings [23]. It is also borne out in figure 8(*b*) by the Φ (135 °C) curve which exhibits a minimum lag at approx. −40 V and turns around as the centroid shifts closer to the Si–SiO_2 interface, followed by the next lower T curve, Φ (82.5 °C). At 40 °C there appear to be no significant effects of decreasing mobility and the radiative recombination is dominated by the increased τ_{p}, which shifts the CDW distribution deeper into the bulk and results in relative phase *lags* with respect to $T = 24$ °C throughout the entire voltage scan. In conclusion, it can be gathered from figure 8 that a significant decrease in minority carrier mobility

as a trade-off to increased lifetime occurs above about 40 °C, with an overall measurable temperature effect on decreasing radiative recombination probability emerging above 82 °C and for applied potentials larger than −70 V.

4. Conclusions

The local internal electric field in an n-type Si MOS diode biased to depletion and inversion was investigated by means of laser infrared photo-carrier radiometry using sideways illumination. Drawing comparisons with direct illumination over a transparent ITO electrode, it was found that frequency-scanned PCR yields information about the spatial separation of the carrier-density-wave statistical (mean) charge centroids below the Si–SiO_2 interface. Minority carrier transport properties have been measured in the presence of the applied external electric field, with a modified PCR theory allowing the extraction of the magnitude of the local internal electric field as 'seen' in the position of the CDW centroid at fixed voltage. Under the combination of increased temperature and applied potential, the sub-interface position of the CDW centroid was found to depend on a trade-off between increased Shockley–Reed recombination lifetime and decreased ambipolar (conductivity) mobility due to thermal scattering with phonons and impurities. The ability of PCR to measure local internal electric fields non-destructively by combining applied bias sweeps and frequency scans appears to be very promising towards the reconstruction of depth profiles of these internal electric fields in active devices, a difficult or impossible task for other existing optical or electrical techniques.

Acknowledgments

AM is grateful to the Alexander von Humboldt Foundation for a Research Award that made this work possible and to Professor Josef Pelzl for his hospitality during the research leave. We wish to acknowledge the valuable technical assistance of Jürgen Gibkes and Dietmar Krüger with computer software and sample holder assembly design.

References

[1] Schroder D K 1997 *IEEE Trans. Electron Devices* **44** 160
[2] Zoth G and Bergholz W 1990 *J. Appl. Phys.* **67** 6764
[3] Antilla O J and Tilli M V 1992 *J. Electrochem. Soc.* **139** 1751
[4] Lagowski J, Edelman P, Kontkiewicz A M, Milic O, Henley W, Jastrzebski L and Hoff A M 1993 *Appl. Phys. Lett.* **32** 3043
[5] Schroder D K 1998 *Semiconductor Material and Device Characterization* 2nd edn (New York: Wiley-Interscience)
[6] Goodman A M 1961 *J. Appl. Phys.* **32** 2550
[7] Jastrzebski L, Milic O, Dexter M, Lagowski J, DeBusk D, Nauka K, Witowski R, Gordon M and Persson E 1993 *J. Electrochem. Soc.* **140** 1152
[8] Park J E, Schroder D K, Tan S E, Choi B D, Fletcher M, Buczkowski A and Kirscht F 2001 *J. Electrochem. Soc.* **148** G411
[9] Mandelis Ed A 1987 *Photoacoustic and Thermal Wave Phenomena in Semiconductors* (New York: North-Holland)
[10] Mandelis A and Hess P (ed) 2000 Semiconductors and Electronic Materials *Progress in Photothermal and Photoacoustic Science and Technology* vol IV (Bellingham WA: SPIE)
[11] Mandelis A 2001 *Diffusion-Wave Fields: Mathematical Methods and Green Functions* (New York: Springer) chapter 9
[12] Salnick A and Mandelis A 1996 *J. Appl. Phys.* **80** 5278
[13] Mandelis A, Williams A and Siu E K M 1988 *J. Appl. Phys.* **63** 92
[14] Mandelis A, Batista J and Shaughnessy D 2003 *Phys. Rev.* B **67** 205208
[15] Rodriguez M E, Mandelis A, Pan G, Nicolaides L, Garcia J A and Riopel Y 2000 *J. Electrochem. Soc.* **147** 687 see table 1 and references therein
[16] Schonecker A, Eikelboom J A, Burgers A R, Lolgen P, Lequijt C and Sinke W C 1996 *J. Appl. Phys.* **79** 1497
[17] McKelvey J P 1969 *Solid State and Semiconductor Physics* (New York: Harper and Row) chapter 10.2
[18] Sze S M 1981 *Physics of Semiconductor Devices* 2nd edn (New York: Wiley) chapter 7
[19] Mandelis A 1982 *Can. J. Phys.* **60** 179–95
[20] Schroder D K 2002 *Math. Sci. Eng.* B **91** 196
[21] Haynes J R and Westphal C W 1952 *Phys. Rev.* **86** 647
[22] Choo S C and Mazur R G 1970 *Solid-State Electron.* **13** 553
[23] Batista J, Mandelis A and Shaughnessy D 2003 *Appl. Phys. Lett.* **82** 4077
[24] Shockley W and Read W T 1952 *Phys. Rev.* **87** 835
[25] Mandelis A 2001 *Diffusion-Wave Fields: Mathematical Methods and Green Functions* (New York: Springer) chapter 6.2
[26] Mette H, Gärtner W W and Loscoe C 1960 *Phys. Rev.* **117** 1491
[27] Ludwig G W and Watters R L 1956 *Phys. Rev.* **101** 1699